EUROPEAN ORGANIZATION FOR NUCLEAR RESEARCH

CERN-EP/80-159
26 August 1980

HYPERNUCLEAR PRODUCTION IN THE (K^-,π^-) REACTION

R. Bertini[1,2], O. Bing[1], P. Birien[3], K. Braune[4], W. Brückner[4], H. Catz[5], A. Chaumeaux[2,3], M.A. Faessler[4], R.-W. Frey[4], D. Garreta[3], T.J. Ketel[4], K. Kilian[4], B. Mayer[3], J. Niewisch[4], B. Pietrzyk[4], B. Povh[4], H.G. Ritter[4] and M. Uhrmacher[4]

[Heidelberg*)-Saclay-Strasbourg Collaboration]

ABSTRACT

Cross-sections for the production of hypernuclei were measured in the reaction $A(K^-,\pi^-)_\Lambda A$ on light and heavy nuclear targets, using a separated K^- beam at the CERN Proton Synchrotron. The pions were detected in the forward direction. The results are compared with cross-sections calculated under the assumption that the reaction took place on a single neutron. The good agreement between the measured and the calculated cross-sections justifies the use of the (K^-,π^-) reaction in order to obtain spectroscopic information on hypernuclei.

(Submitted to Nuclear Physics A)

---

*) This work was supported in part by the Bundesministerium für Forschung und Technologie, Bonn, Germany.

1) CRN, Strasbourg, France.

2) CERN Associate.

3) Département de Physique Nucléaire, CEN Saclay, France.

4) Max-Planck-Institut für Kernphysik, Heidelberg, Germany, and Physikalisches Institut der Universität, Heidelberg, Germany.

5) CERN Fellow.

1. INTRODUCTION

The strangeness exchange reaction (K^-,π^-) on nuclei has played a central role in hypernuclear spectroscopy. This is largely due to its kinematical properties, which are very suitable for the forming of hypernuclei under well-defined conditions. For kaon momenta around 500 MeV/c and forward emitted pions the recoil of the produced Λ particle is small compared with the Fermi momentum of the nucleons in the nucleus[1,2]. The Λ particle is expected to occupy either the same orbit as the neutron on which the reaction took place, or one of the neighbouring orbits. It has been found that the dominant transitions observed in the (K^-,π^-) reaction are understood, at least qualitatively, in accordance with this expectation[3].

The use of the strangeness exchange reaction as a tool for hypernuclear spectroscopy requires, however, that the transition probabilities in the (K^-,π^-) reaction to the hypernuclear states give reliable information on the structure of these states. This is so only if the reaction occurs on a single neutron -- a one-step reaction -- without any additional interaction of either the incoming K^- or the outgoing π^- with the rest of the nucleus. In view of the strong absorption of pions and kaons in the nucleus, it is certainly not evident *a priori* whether or not distortions in the (K^-,π^-) reaction on nuclei can be sufficiently well taken into account theoretically.

The aim of this paper is thus:

i) to present the results of the systematic study of production cross-sections for Λ hypernuclei in the (K^-,π^-) reaction on light and heavy nuclear targets,

ii) to compare these cross-sections with calculations for the hypernuclear production in a one-step process, taking into account the distortion in the (K^-,π^-) reaction, and

iii) to show that the agreement of the measured and the calculated cross-sections is sufficiently good to allow a detailed study of the configurations of the low-lying excited hypernuclear states, by using the strangeness exchange reaction on nuclei.

2. EXPERIMENT

The spectra of the Λ hypernuclei produced in the (K^-,π^-) strangeness exchange reaction were obtained using the missing-mass technique. For each event the momentum of the incoming kaon and of the emitted pion had to be analysed, as well as the relative angle between the trajectories of those particles. The mass of the hypernuclear system could then be calculated, using the known masses of the target, kaon, and pion. In this section we describe in detail the experimental set-up and the off-line analysis procedures which were necessary to produce the hypernuclear spectra.

2.1 The kaon beam

The momenta of the incoming kaons were chosen between 640 MeV/c and 790 MeV/c by means of the separated kaon beam k_{22} at the CERN Proton Synchrotron (PS). The beam line is shown schematically in fig. 1. Kaons from the production target are refocused to give an achromatic focus (3.5 × 0.8 cm^2 in size) on the experimental target T. The total length of the beam line, including the part used as the kaon spectrometer, was only 18 m. Under normal operation, with about 1.3×10^{12} protons of 26 GeV/c on a 3 cm long tungsten production target, 2×10^4 kaons of 720 MeV/c reached the experimental target. A sufficient separation between kaons and pions was achieved, using a 3 m long electrostatic separator and a mass-slit formed by a set of uranium blocks which were shaped according to the calculated kaon beam profile in the region of the slits. The π^-/K^- ratio of about 12 at the experimental target can be considered as excellent for such a short high-intensity beam. The k_{22} beam was designed to have an angular acceptance of 9 msr and to transport a momentum bite of only 3%. The momentum of the beam particles could be determined with sufficient precision, using just the last part of the beam transport system (in fig. 1 form P1 to P2) as the kaon spectrometer.

2.2 The pion spectrometer

Forward produced pions in the experimental target were analysed in the specially designed magnetic spectrometer SPES II of Saclay, which has been described

in detail elsewhere[4]. The angular acceptance of the spectrometer was about 40 msr and the accepted momentum bite ±18%. It could rotate around the target axis from 0° to 30°, moving on six air cushions. SPES II was already tested at Saclay and found to have a resolution of better than 0.5 MeV/c at 700 MeV/c beam momentum[4]. The main difficulty in the present experiment consisted in extending the spectrometer programs to the bigger target size used. A correction procedure was found which gave the same good resolution over the whole acceptance. To obtain an almost flat acceptance (from −14% to +14% $\Delta p/p$) the measured angles were cut by software to 20 msr ($\theta \leq 50$ mrad, $\phi \leq 100$ mrad).

2.3 Identification of the (K^-,π^-) reaction

The kaons and pions in the two spectrometers were identified by measuring their time of flight (TOF) and by the use of two Čerenkov threshold counters. The kaon TOF through the first spectrometer was measured between P1 and P2, and independently between H1 and P2. Owing to the high counting rate in the mass-slit region the entrance timing counter P1 consisted of three separate scintillation counters. The beam pions were vetoed by a liquid-hydrogen (LH_2) Čerenkov counter $\check{C}_1$ in front of the target T. Pions behind the reaction target were identified by the TOF through the spectrometer SPES II between the counter P2 and the exit scintillation counter hodoscope H2. Owing to the large acceptance of SPES II it was necessary to calculate to first order the track length through the spectrometer to obtain the corrected TOF for the pions. The second LH_2 counter $\check{C}_2$ just behind the target was used to identify pions. Its task was to dispose of passing kaon events already in the on-line trigger. Owing to the high counting rate in the entrance counters P1 and H1 (about 3.5×10^6 counts/PS pulse) there was a great probability of having double particle events, in which a pion after triggering was lost and a following pion simulated the kaon TOF at the target. The scintillators of the entrance timing counter P1 and the 50 scintillator slabs of the entrance hodoscope H1 were only a few centimetres apart geometrically. The measured TOF to the target counter P2 and the multiplicity in the entrance hodoscope H1 were used to rule out most of these double particle events.

2.4 Target region

Figure 2 shows the target region in more detail. A vacuum box V houses the target and the twin Čerenkov counters ($\check{C}_1$ and $\check{C}_2$) with LH_2 as radiator. The refractive index of LH_2 is n = 1.112, which allows discrimination between pions and kaons in a momentum range from 300 to 1000 MeV/c. The two radiator cells are made out of 170 μm thick mylar. Additional layers of aluminized mylar, with a total thickness of about 400 μm, were used for thermal insulation. This amount of mylar near the reaction target caused some $^{12}_{\Lambda}C$ production, which had to be considered in determining the integrated cross-section, especially for heavy targets. The two radiator cells (4 cm in diameter) contain a thin inclined mirror foil M to improve the light collection in the direction of the cylinder axes. Each single cell was viewed by two photomultiplier tubes. On the average, 8 photoelectrons were collected per radiator cell for a passing pion. The inefficiency for pion identification therefore was less than 5×10^{-4}. The target itself was mounted either directly inside the vacuum box, to avoid additional material near the target, or outside the vacuum in a small housing, which allowed target changes without breaking the high vacuum needed to make the thermal insulation of the LH_2 cells. The targets had a size of 2 × 5 cm and their thickness was about 2 g/cm^2. They were surrounded by a scintillation counter for detecting hypernuclear decay (see also Section 2.7).

2.5 Measurement of particle coordinates and vertex reconstruction

To determine the momenta, the interaction vertex, and the reaction angle of the particles, it is necessary to measure their trajectories. To minimize the effects of straggling in the position-sensitive counters they have to be as close as possible to a focal plane. At the first focal plane -- the slit region -- we determined the particles' position with the help of the scintillator hodoscope H1. Owing to the high counting rate at this place, the use of wire chambers was not possible. The hodoscope was installed directly between the blocks of the mass and momentum slits in order to be near to the focal plane. It consisted of 30 hodoscope slabs, each 3 mm wide and 4 mm thick, which measured the position of a

particle in the horizontal x-plane, and of 20 additional slabs, which measured the position in the vertical y-plane. The counting rate in these counters was 90% due to beam particles and 10% due to a flux of neutrons with low momentum from the beam dump. This favourable background condition was achieved by elaborate shielding of the counters.

Near the reaction target we used the four multiwire proportional chambers (MWPCs) W2-W5 for the vertex reconstruction. Their wire spacing was 1 mm and the read-out was performed by the RMH system[5] developed at CERN. These chambers around the target were required to give unique information. The calculated tracks in front of and behind the target had to meet inside the target volume with an accuracy of better than 2 mm. In about 30% of the cases one out of eight planes was missing. Most of the events, however, could be recovered by the following procedure. The interaction point was assumed to be in the centre of the target. Then the track position in the chamber with the missing plane was calculated, and it was checked if in the working plane a wire had fired within 2 mm of the calculated position. Only such events, in addition to the ideal 8-plane events, were accepted in the analysis.

In the exit of the pion spectrometer, we used the set of three large chambers of SPES II (W6-W8), described in detail elsewhere[6]. As the minimum condition, two of the three chambers were required to have unique coordinates. These exit coordinates were used to calculate the momentum in the pion spectrometer with its known magnetic field. They also allowed a track reconstruction back to the reaction target. A comparison with the measured coordinates in the chambers W4 and W5 at the SPES II entrance ruled out most of the kaon decays in the SPES II volume. The total evaluation efficiency of all chambers used was about 80%.

The large angular acceptance of SPES II of 20 msr allowed, even with the spectrometer adjusted to 0°, the determination of the interaction point along the beam axis with an average spatial resolution of 1.5 cm. This was good enough to distinguish between events stemming from reactions in the target and those from reactions in the windows or the LH_2 counters. It is demonstrated in fig. 3 where

the hypernuclear mass spectrum, obtained in the (K^-,π^+) reaction on a ^{9}Be target, is displayed versus the beam axis. This special reaction was chosen because via the $p(K^-,\pi^+)\Sigma^-$ reaction only the production of Σ^- particles on protons can occur. Now the protons of the LH_2 counters themselves act as additional targets. As the production of Σ^- particles on free protons is well separated in energy from the production on the protons of the ^{9}Be nuclei[7], the positions of the LH_2 counters and the target can easily be recognized.

2.6 Calibration of the spectrometers

The pion spectrometer SPES II has a well-known magnetic field and a momentum resolution in the momentum range of this experiment of about 0.5 MeV/c. It was thus natural to perform the calibration and optimization of the momentum resolution of the kaon spectrometer with the help of SPES II. The momentum of the beam particles passing through the kaon spectrometer was analysed by SPES II. With this passing particle data the coefficients of a linear expansion in coordinates and angles at the focal planes were determined by optimizing the momentum resolution. Using these coefficients the kaon momentum was calculated from the x coordinates measured with 3 mm resolution in the entrance scintillation hodoscope H1, and from the (x,y) coordinates at the target position measured with 1 mm resolution in the two chambers W2 and W3 in front of the target which also gave the angles of the particle tracks in the target. At 720 MeV/c a resolution of 2.0×10^{-3} FWHM was achieved close to the expected value for the kaon spectrometer. In the (K^-,π^-) reactions the thickness of the targets determined the energy resolution, mainly because of straggling both in the target and in the particle identification counters before and behind the target. Depending on the thickness of the target used, an over-all energy resolution of 1.5 to 3 MeV was thus obtained in the spectra.

2.7 Background rejection

The most difficult problem in the (K^-,π^-) spectroscopy is to deal correctly with the high beam-pion background and with pions from the kaon decay in flight. In this experiment the high efficiency of the two LH_2 counters, together with the TOF in the first spectrometer, suppressed almost all the beam pions and restricted

the space where the decay of a kaon could not be identified by the trigger to the distance of roughly 5 cm between the radiator cells. With 2×10^4 kaons at the reaction target only 2-3 events passed the hardware trigger and were recorded on magnetic tape.

The main decay modes of the kaon are the two-body decays $K^- \rightarrow \mu^- + \nu$ (63.5%) and $K^- \rightarrow \pi^- + \pi^0$ (21.2%). In a two-dimensional plot of the reaction angle versus the hypernuclear mass, only the latter appears in our mass range as a sharp curved line (figs. 4-1a, b), whereas hypernuclear events give straight lines owing to the much higher mass of the system. Calculating a missing-mass spectrum of the events with the assumption of $(K^- \rightarrow \pi^- + \pi^0)$ decay transforms the curved line into a sharp peak of 4 MeV width on the mass axis at the position of the π^0 (figs. 4-2a, b). In the final spectra these events were cut out. For heavy hypernuclei the kinematical curve of the $K^- \rightarrow \pi^- + \pi^0$ decay comes close to the hypernuclear events at higher reaction angles (> 80 mrad), so that in these spectra the region of hypernuclear states bound by more than 15 MeV can be obscured by such decay events. On the other hand, these $(K^- \rightarrow \pi^- + \pi^0)$ events gave an ideal possibility to do an absolute mass calibration of the hypernuclear spectra. Pions from this decay channel have higher momenta than most pions from Λ hypernuclear production. As the mass of the π^0 is known, the momentum of the π^- can be well adjusted. In addition, the reaction $p(K^-,\pi^-)\Sigma^+$ which occurred on the protons of the LH_2 counters (figs. 4-3a, b) -- even with low cross-section at 720 MeV/c -- gave a second calibration line, if events were selected which had their interaction point in one of the LH_2 cells. Pions from this reaction have lower momenta than most of the pions from Λ hypernuclear production. Therefore the mass of the hypernuclear system could be determined with an uncertainty of ± 0.5 MeV.

Two additional decay channels of the kaon also contributed in the measured momentum range: the three-body decays $K^- \rightarrow \mu^- + \nu + \pi^0$ with a branching ratio of 3.2%, and the $K^- \rightarrow e^- + \nu + \pi^0$ decay with a branching ratio of 4.82%. Our set-up could not distinguish between pions, muons, and electrons in the exit of the pion

spectrometer, whereas such decays occurring between the two LH_2 counters fulfilled all trigger conditions for a (K^-,π^-) reaction. To estimate the influence of these decays on the hypernuclear spectra, the shape of the muon or electron momentum distribution as well as the intensity normalized to 10^9 kaons was generated by a Monte Carlo procedure. We found a good agreement with the background observed in the Λ hypernuclear spectra at the region of high excitation, but we cannot exclude contributions from other channels (e.g. multistep processes). In the evaluation procedure, this background could only be reduced by using the information about the hypernuclear decay. The target was surrounded by a scintillation counter. In the case of Λ hypernuclear production this counter detected the decay products: pions and/or heavy nuclear fragments. Thirty to forty per cent of the hypernuclear events were accompanied by a high pulse in this counter, which is roughly in agreement with the solid angle and the efficiency of this counter. Imposing this condition, the hypernuclear spectra look much cleaner and the high excitation background is significantly reduced. But as this condition might be selective to special decay modes of the hypernucleus, these spectra were not used for the cross-section evaluation.

3. RESULTS

3.1 Hypernuclear spectra

Using the known masses of the kaon, pion, and the target, together with the measured momenta of the kaon and pion and the measured reaction angle θ, the mass of the hypernuclear system M_{Hy} could be calculated:

$$M_{Hy}^2 = E_{tot}^2 - p_K^2 + p_\pi^2 - 2(E_{tot})\, E_\pi + p_K p_\pi \cos\theta \ , \qquad (1)$$

where $E_{tot}^2 = (p_K^2 + m_K^2)^{\frac{1}{2}} + m_{target}$ is the total energy in the system. Historically the Λ-binding energy scale has been widely used to present hypernuclear spectra. This scale is calculated as

$$B_\Lambda = m_{target} - m_n + m_\Lambda + B_n - M_{Hy} \ . \qquad (2)$$

B_n is the binding energy of the last neutron in the target and m_i the mass of the indexed particle. A state with a positive B_Λ value corresponds to a lambda particle bound to the core-nucleus ground state. In order to compare the (K^-,π^-) reaction on different nuclei the transformation energy

$$M_{Hy} - M_A = M_{Hy} - m_{target} \tag{3}$$

was found to be useful in the interpretation of the spectra. On this scale the higher excitation of the hypernuclear system corresponds to a higher transformation energy. The spectra of fig. 5 are plotted on this scale; in addition the binding energy B_Λ is given at the bottom of each single spectrum. Figure 5 displays spectra measured in the (K^-,π^-) strangeness exchange reaction on carbon[8], aluminium, vanadium, and bismuth. In all spectra the predominant feature is an enhancement starting at about B_Λ = 0 MeV and reaching up to about 50 MeV excitation. In addition, well separated peaks at $B_\Lambda \approx 0$ are clearly observed. This is one of the most encouraging results as it guarantees the use of the strangeness exchange reaction for quantitative measurements in hypernuclear spectroscopy.

At $B_\Lambda \approx 0$ MeV the transitions to the hypernuclear states presumably belong to the one-step strangeness exchange reaction, where just one neutron in the nucleus is converted into a lambda particle, while the rest of the nucleus is left unchanged. In the qualitative picture of the hypernuclear production we can expect that mainly the less bound neutrons of the last nuclear shells will be transformed into Λ particles. The Λ particle is then produced either in the orbit of the neutron on which the strangeness exchange reaction took place -- recoilless Λ production -- or in one of the neighbouring orbits. Using the simple model we can expect that with increasing kaon momentum the recoil to the Λ particle is used to produce the Λ in a different orbit. In addition, heavier nuclei with higher level densities provide more possible states. In contrast, the recoilless Λ production will dominate, especially for the lighter hypernuclei and for kaon momenta near to the "magic" momentum of 530 MeV/c, where the Λ particle gets no recoil at all. Such a behaviour can be seen clearly in fig. 5. More elaborate calculations on the probability for recoilless Λ production can be found in a paper by Povh[9].

The dominant peak at $B_\Lambda \approx 0$ MeV in each of the four spectra of fig. 5 is therefore ascribed to the hypernuclear 0^+ state, where a neutron of the last nuclear shell is replaced by a Λ particle with the same quantum numbers. The structure of these states is indicated in the figure. For carbon, aluminium, and vanadium a smaller bound peak is also clearly resolved. In analogy with the already analysed hypernuclear spectra[8,10,11] of ${}^{12}_{\Lambda}C$, ${}^{16}_{\Lambda}O$, ${}^{32}_{\Lambda}S$, and ${}^{40}_{\Lambda}Ca$, this peak is ascribed to the hypernuclear 1^- state, where a neutron of the last shell is transformed into the Λ particle, but where the Λ particle occupies the neighbouring deeper lying shell. For ${}^{12}_{\Lambda}C$, measurements of the angular distribution of both peaks[8,12] proved the spin assignment to these states. Additional states will be found in the broad unresolved structure, which reaches 50 MeV excitation energy in the hypernuclear spectra. For heavy hypernuclei this structure becomes dominant. The background seen in the spectra of fig. 5 still contains, after all cleaning procedures, events from the kaon decay in the target region as well as possible multistep processes.

3.2 Cross-sections

Much effort was made to measure the transitions in the (K^-,π^-) reaction at sufficiently high excitations so as to enable a good estimate of the integrated cross-section. The main problem lies in distinguishing between the one-step process and the background in the region of high excitation, but for heavier hypernuclei in addition a background is present around $B_\Lambda = 0$ MeV, as can be seen from fig. 5. The most simple assumption is a background which rises linearly from $B_\Lambda = 15$ MeV up to $B_\Lambda = -50$ MeV. Such a background is indicated in fig. 5 as the straight line in each spectrum. It will lead to a lower limit of the integrated production cross-section $(d\sigma/d\Omega)^{0^\circ}_{min}$. In the following, some of the background contributions are accounted for in more detail. The hypernuclear spectrum may contain some background from the $K^- \to \pi^0 + \pi^-$ decay at higher reaction angles in the region between $B_\Lambda = 15$ MeV and $B_\Lambda = 0$ MeV (see figs. 4-1a, b). As the acceptance of SPES II limits the reaction angles to $\Theta \leq 120$ mrad, this background disappears naturally at about $B_\Lambda = 0$ MeV. Therefore we assumed a linear decreasing

background, which goes to zero at B_Λ = 0 MeV. The second main contribution is the three-body decay of kaons, as described earlier. It causes a flat distribution of events, which rises to higher excitation energies in the hypernuclear spectra. As the spectra are flat above B_Λ = -50 MeV, except for Σ production[13], we assume there are only background events at B_Λ = -50 MeV. Near B_Λ = 0 MeV we have no good estimate of the amount of this type of background, especially as contributions from multistep processes may appear. So finally a background was subtracted, which decreased from B_Λ = 15 MeV to B_Λ = 0 MeV to zero and increased again linearly to B_Λ = -50 MeV. This subtraction leads to an upper limit of the integrated production cross-section $(d\sigma/d\Omega)^{0^\circ}_{max}$.

The cross-sections for the heavier ($A \geq 40$) targets had to be corrected for the $^{12}_{\Lambda}C$ content in the spectra, which was calculated from the amount of ^{12}C near the target and the measured cross-section for $^{12}_{\Lambda}C$.

A further correction had to be applied to the cross-section, as the (K^-,π^-) events had to satisfy certain conditions so as to be accepted in the analysis. The rejected events, however, also have to be taken into account in the cross-section determination.

In table 1 the experimental cross-sections for the different targets are given as the average value of $(d\sigma/d\Omega)^{0^\circ}_{min}$ and $(d\sigma/d\Omega)^{0^\circ}_{max}$, defined above. The errors contain the uncertainty in the background definition, the ^{12}C contamination, and the event rejections made in the analysis.

Many authors[11,14-16] have calculated the effective number of neutrons N_{eff} which contribute to the one-step strangeness exchange reaction for 0° production. N_{eff} is defined by the relation:

$$(d\sigma/d\Omega)_{\theta=0^\circ} = N_{eff}(d\sigma/d\Omega)_{K^-N\to\Lambda\pi^-} \qquad (4)$$

and is calculated, for instance, by Dalitz and Gal[15] using closure relations. Bouyssy[11,17], on the other hand, calculates the cross-section for hypernuclear states with simple particle-hole configurations up to 60 MeV excitation. In table 1 different theoretical predictions of N^{tot}_{eff} are given. They all show an increasing N_{eff} with higher mass number A. If one describes this dependence by

A^n, the different predictions range from n = 0.3 [15] to n = 0.5 [16]. The calculations of Bouyssy[17] allow in addition the extraction of the amount of recoilless Λ production in N_{eff}^{tot}, which is also given in table 1: N_{eff}^{rl} is constant over the whole mass range and is about equal to one. This is in agreement with the experiment, where the recoilless peaks tend to disappear with increasing target mass (fig. 5) in the broad structure of other unresolved transitions.

For a direct quantitative comparison between the calculations and the experiment, the cross-sections for the elementary reaction $K^- + n \rightarrow \Lambda + \pi^-$ have to be known at the different momenta chosen in the experiment. Only a few data exist[18,19] from bubble chamber experiments which are listed in table 2. From the data of Hepp et al.[19] we assumed for all three different kaon momenta a constant value of $(d\sigma/d\Omega)_{cm}^{0°} = 0.95 + 0.13$ mb/sr in the centre-of-mass system. After the transformation to the laboratory system the elementary cross-sections $(d\sigma/d\Omega)_{lab}^{0°}$ are given in the last column of table 2. They were used to calculate N_{eff}^{tot} from the experimental cross-sections[15-17]. In fig. 6 the measured integrated cross-sections are plotted together with the calculations of Bouyssy[17]. Owing to the uncertainty in the elementary cross-section, the theoretical curve may shift by ±15%. As we can see, the experimental values and the calculations agree fairly well.

3.3 Discussion

The measured integrated cross-sections for hypernuclear production can be well reproduced using closure relations as well as distorted wave impulse approximation calculations summing up the contributions to the single Λ-particle-neutron hole states. The summation has to extend to the states up to 70 MeV excitation. Previously believed disagreement between the calculations and the measurement[3] was at least partially due to the fact that hypernuclear spectra were measured only up to 30 MeV excitation.

Distorted wave impulse approximation calculations for transition probabilities to hypernuclear states with simple particle-hole configurations give a

rather successful account of the data. The cross-sections can be calculated and the shape of the Λ hypernuclear spectra is reproduced. Furthermore, the angular distributions of different states at small[20,21] and large[21] angles can be described successfully.

The fair agreement between the experiment and the theoretical description leads to the conclusion that we understand the main features of the hypernuclear production in the (K^-,π^-) reaction on nuclei: the one-step process is a good approximation if the population of low-excited hypernuclear states is to be calculated and the relative transition probabilities to isolated states yield reliable information on the hypernuclear configuration.

We wish to thank V. Soergel and J. Thirion for many stimulating discussions concerning the experiment and A. Bouyssy, H.C. Chiang, R.H. Dalitz, A. Gal, J. Hüfner, H. Pirner, H.A. Weidenmüller and W. Weise for many discussions concerning the results. A. Bouyssy kindly gave us his calculations before publication. The k_{22} beam line was designed by M. Ferro-Luzzi of CERN. The continuous support of our technician, Z. Kenesei, and members of the Département de Physique Nucléaire at CEN, Saclay, of the CERN MPS Group, and the Hydrogen Group under L. Mazzone at CERN, was essential for the success of the experiment.

REFERENCES

1) M.I. Podgoretskii, Zh. Exp. Teor. Fiz 44 (1963) 695 [Engl. transl: Sov. Phys.-JETP 17 (1963) 470].

2) H. Feshbach and A.K. Kerman, Preludes in theoretical physics (North Holland, Amsterdam, 1965), p. 260.

3) W. Brückner, B. Granz, D. Ingham, K. Kilian, U. Lynen, J. Niewisch, B. Pietrzyk, B. Povh, H.G. Ritter and H. Schröder, Phys. Lett. 62B (1976) 481.

4) E. Aslanides, R. Bertini, O. Bing, P. Birien, B. Bricaud, F. Brochard, H. Catz, J.M. Durand, J.C. Faivre, D. Garreta, Ph. Gorodetzky, F. Hibou, J. Pain and J. Thirion, *in* Abstracts of papers submitted to the 7th Int. Conf. on High Energy Physics and Nuclear Structure, Zurich, 1977 (SIN, Villigen, 1977), p. 376.

5) J.B. Lindsay, C. Millerin, J.C. Tarlé, H. Verweij and H. Wendler, Nucl. Instrum. Methods 156 (1978) 329.

6) R. Chaminade, J.M. Durand, J.C. Faivre and J. Pain, Nucl. Instrum. Methods 118 (1974) 477.

7) W. Brückner, M.A. Faessler, T.J. Ketel, K. Kilian, J. Niewisch, B. Pietrzyk, B. Povh, H.G. Ritter, M. Uhrmacher, P. Birien, H. Catz, A. Chaumeaux, J.M. Durand, B. Mayer, R. Bertini, O. Bing and A. Bouyssy, *in* Proc. Kaon Factory Workshop, Vancouver, 1979 (TRIUMF, Vancouver, 1979: TRI-79-1), p. 136.

8) W. Brückner, M.A. Faessler, T.J. Ketel, K. Kilian, J. Niewisch, B. Pietrzyk, B. Povh, H.G. Ritter, M. Uhrmacher, P. Birien, H. Catz, A. Chaumeaux, J.M. Durand, B. Mayer, J. Thirion, R. Bertini and O. Bing, Phys. Lett. 79B (1978) 157.

9) B. Povh, Z. Phys. A279 (1976) 159.

10) R. Bertini, O. Bing, P. Birien, W. Brückner, H. Catz, A. Chaumeaux, J.M. Durand, M.A. Faessler, T.J. Ketel, K. Kilian, B. Mayer, J. Niewisch, B. Pietrzyk, B. Povh, H.G. Ritter and M. Uhrmacher, Phys. Lett. 83B (1979) 306.

11) A. Bouyssy, Phys. Lett. 84B (1979) 41.

12) R.E. Chrien, M. May, H. Palevsky, R. Sutter, P. Barnes, S. Dytman, D. Marlow, F. Takeutchi, M. Deutsch, R. Cester, S. Bart, E. Hungerford, T.M. Williams, L.S. Pinsky, B.W. Mayes and R.L. Stears, Phys. Lett. 89B (1979) 31.

13) R. Bertini, O. Bing, P. Birien, W. Brückner, H. Catz, A. Chaumeaux, J.M. Durand, M.A. Faessler, T.J. Ketel, K. Kilian, B. Mayer, J. Niewisch, B. Pietrzyk, B. Povh, H.G. Ritter and M. Uhrmacher, Phys. Lett. 90B (1980) 375.

14) J. Hüfner, S.Y. Lee and H.A. Weidenmüller, Nucl. Phys. A234 (1974) 429.

15) R.H. Dalitz and A. Gal, Phys. Lett. 64B (1976) 154.

16) G.N. Epstein, F. Tabakin, A. Gal and L.S. Kisslinger, Phys. Rev. C17 (1978) 1501.

17) A. Bouyssy, private communication, to be published.

18) R. Armenteros, P. Baillon, P. Lexa, A. Minten, K.H. Nguyen, E. Pagiola, V. Pelosi, R. Barloutaud, F. Bigata, M. Crozon, C. Louedec, J.L. Narjoux and F. Pierre, Nucl. Phys. B18 (1970) 425.

19) V. Hepp, O. Braun, H.J. Grimm, H. Ströbele, C. Thöl, T.J. Thouw, D. Capps, F. Gandini, C. Kiesling, D.E. Plane and W. Wittek, Nucl. Phys. B115 (1976) 82.

20) H.C. Chiang and J. Hüfner, Phys. Lett. 84B (1979) 393.

21) C.B. Dover, A. Gal, G.E. Walker and R.H. Dalitz, Phys. Lett. 89B (1979) 26.

Table 1

Comparison of cross-sections

Nucleus	p_{K^-} (MeV/c)	Target thickness (g/cm^2)	Experimental values		Calculated values			
			$\left(\frac{d\sigma}{d\Omega}\right)^{0°}$ (mb/sr)	N_{eff}^{tot} a)	Ref. 17 N_{eff}^{tot}	Ref. 17 N_{eff}^{rl}	Ref. 15 N_{eff}^{tot}	Ref. 16 N_{eff}^{tot}
^{6}Li	790	1.13	3.6 ± 1.0	1.5 ± 0.4	1.50	1.16		
^{7}Li	720	1.28	3.4 ± 1.0	1.5 ± 0.4	1.58	1.14		
^{7}Li	790	1.28	4.4 ± 1.2	1.8 ± 0.5	1.58	1.14		
^{9}Be	720	2.22	3.5 ± 1.0	1.5 ± 0.4	1.86	1.28	0.43	
^{9}Be	790	2.22	3.8 ± 0.9	1.6 ± 0.4	1.86	1.28	0.43	
^{12}C	720	2.00	3.8 ± 1.0	1.7 ± 0.4	1.67	1.08	0.53	1.80
^{16}O	720	1.50	3.9 ± 1.3	1.7 ± 0.6	1.97	1.21	0.57	
^{27}Al	720	3.78	7.8 ± 2.3	3.5 ± 1.0	2.35	1.10		
^{32}S	720	2.69	5.6 ± 1.6	2.5 ± 0.7	2.52	1.17	0.67	
^{40}Ca	790	1.55	4.9 ± 2.0	2.1 ± 0.8	2.40	1.04	0.69	3.54
^{51}Va	720	1.94	3.0 ± 1.4	1.3 ± 0.6	2.70	1.15		
^{89}Y	720	1.61	4.8 ± 3.9	2.1 ± 1.7	3.91	1.08		
^{209}Bi	640	3.33	10.5 ± 3.7	5.0 ± 1.8	7.00	1.01		

a) Calculated from $(d\sigma/d\Omega)^{0°}_{lab}$ from Table 2.

Table 2

Cross-sections for the elementary reaction

p_{K^-} (MeV/c)	Ref. 18 $\left.\frac{d\sigma}{d\Omega}\right\|^{0°}_{cm}$ (mb/sr)	Ref. 19 $\left.\frac{d\sigma}{d\Omega}\right\|^{0°}_{cm}$ (mb/sr)	Adopted value $\left.\frac{d\sigma}{d\Omega}\right\|^{0°}_{cm}$ (mb/sr)	$\left.\frac{d\sigma}{d\Omega}\right\|^{0°}_{lab}$ (mb/sr)
640	-	0.847 + 0.144	0.95 + 0.13	2.11 + 0.29
720	1.10 + 0.26	0.980 + 0.124	0.95 + 0.13	2.26 + 0.31
790	1.26 + 0.30	0.937 + 0.142	0.95 + 0.13	2.39 + 0.33

Figure captions

Fig. 1 : Experimental set-up. Kaon and pion momenta are analysed by means of a magnetic system. The particle trajectories are determined by the hodoscopes H1 and H2 and the wire chambers W1-W8. Kaons and pions are identified by the liquid hydrogen Čerenkov counters Č1 and Č2 at the target position and by time-of-flight measurements between the scintillation counters P1, P2, and H2.

Fig. 2 : Details of the target region. After passage of a kaon through the wire chamber W3 the scintillation counter P2 is used to give the TOF information in the kaon spectrometer and to define the beam size. A high-vacuum box V contains the target T and the two Čerenkov counters Č1 and Č2, which are filled with LH_2. A mirror M in each cell directs the light into the two phototubes looking at the cell.

Fig. 3 : Spatial resolution along the beam axis. The lower part of the figure shows size and position of the radiator cells Č1 and Č2 and the target itself. In the upper part the hypernuclear mass spectrum from the (K^-,π^+) reaction on ^9Be is displayed along the beam axis in the same scale. Reactions on the free protons of the LH_2 counters are well separated from the reactions on the bound protons in the ^9Be nuclei.

Fig. 4 : Mass calibration in the (K^-,π^-) reaction. A sample of events from the (K^-,π^-) reaction on ^6Li at 790 MeV/c was treated with different assumptions about the reaction which had occurred. Figures 4-1a, 4-2a, 4-3a show the two-dimensional plots of the reaction angle versus a mass scale in MeV, obtained with the indicated assumption on the reaction type. Figures 4-1b, 4-2b, 4-3b are the corresponding projections on the mass axis. In figs. 4-1a and b the production of $^6_\Lambda Li$ is assumed. The curved line from the $K^- \rightarrow \pi^- + \pi^0$ decay which appears in Fig. 4-1a is transformed to a straight line in fig. 4-2a,

if one calculates with the correct kinematics. Figure 4-2b gives a peak at the mass of the π^0 and can be used to calibrate the mass spectrum. In the same way the reaction $K^- + p \rightarrow \Sigma^+ + \pi^-$ is treated to obtain the second calibration line in fig. 4-3b.

Fig. 5 : Different Λ-hypernuclear spectra obtained in the (K^-,π^-) reaction. The spectra are plotted against a common transformation energy scale $(M_{Hy} - M_A)$ which is indicated at the top of the figure. In addition the binding energy scale B_Λ is given for each single spectrum. The solid line through the data points is shown to guide the eye. The dotted line in each of the four spectra corresponds to the calculation of ref. 17 and shows the part of the spectrum which is due to recoilless Λ production. The straight line indicates the first type of background, which was assumed in order to calculate the integrated cross-sections. This type leads to the minimum value.

Fig. 6 : The integrated cross-sections $(d\sigma/d\Omega)^{0^\circ}$ for the Λ-hypernuclear production in the (K^-,π^-) reaction are plotted versus the mass number A of the target nucleus. The calculations of Bouyssy[17] are indicated by the crosses, assuming the elementary cross-section given in table 2. The dotted line serves to guide the eye along these calculated values.

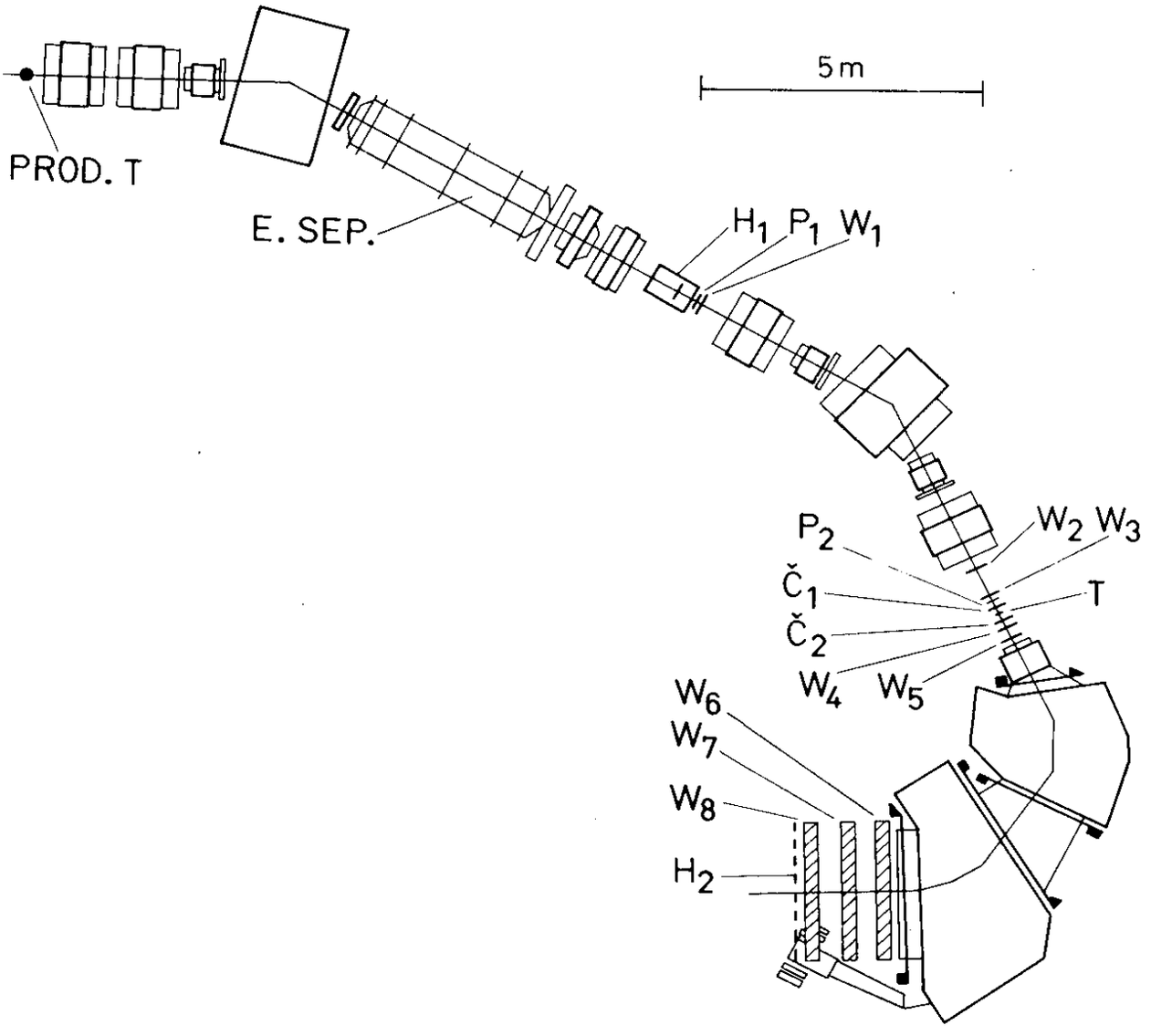

Fig. 1

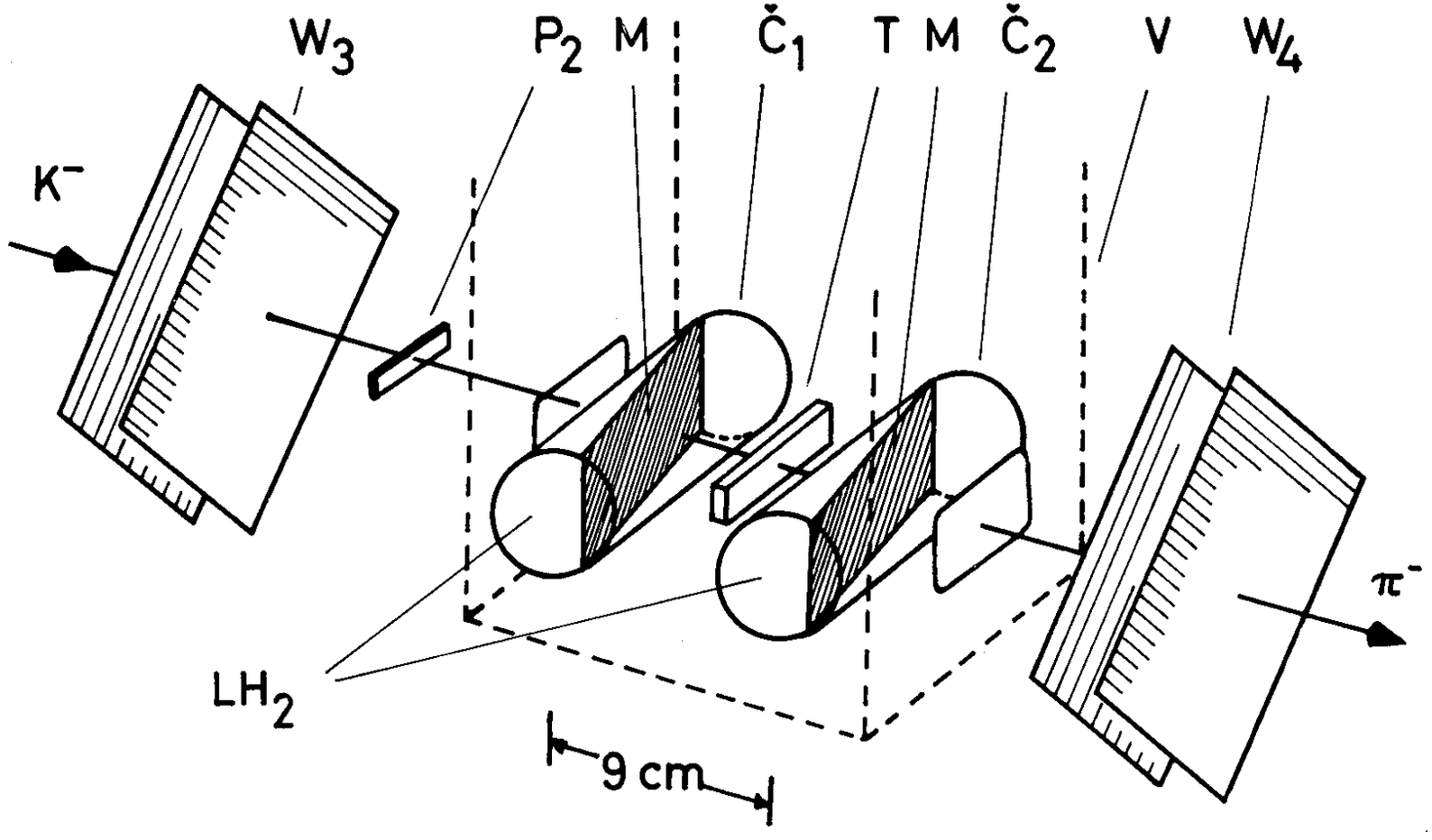

Fig. 2

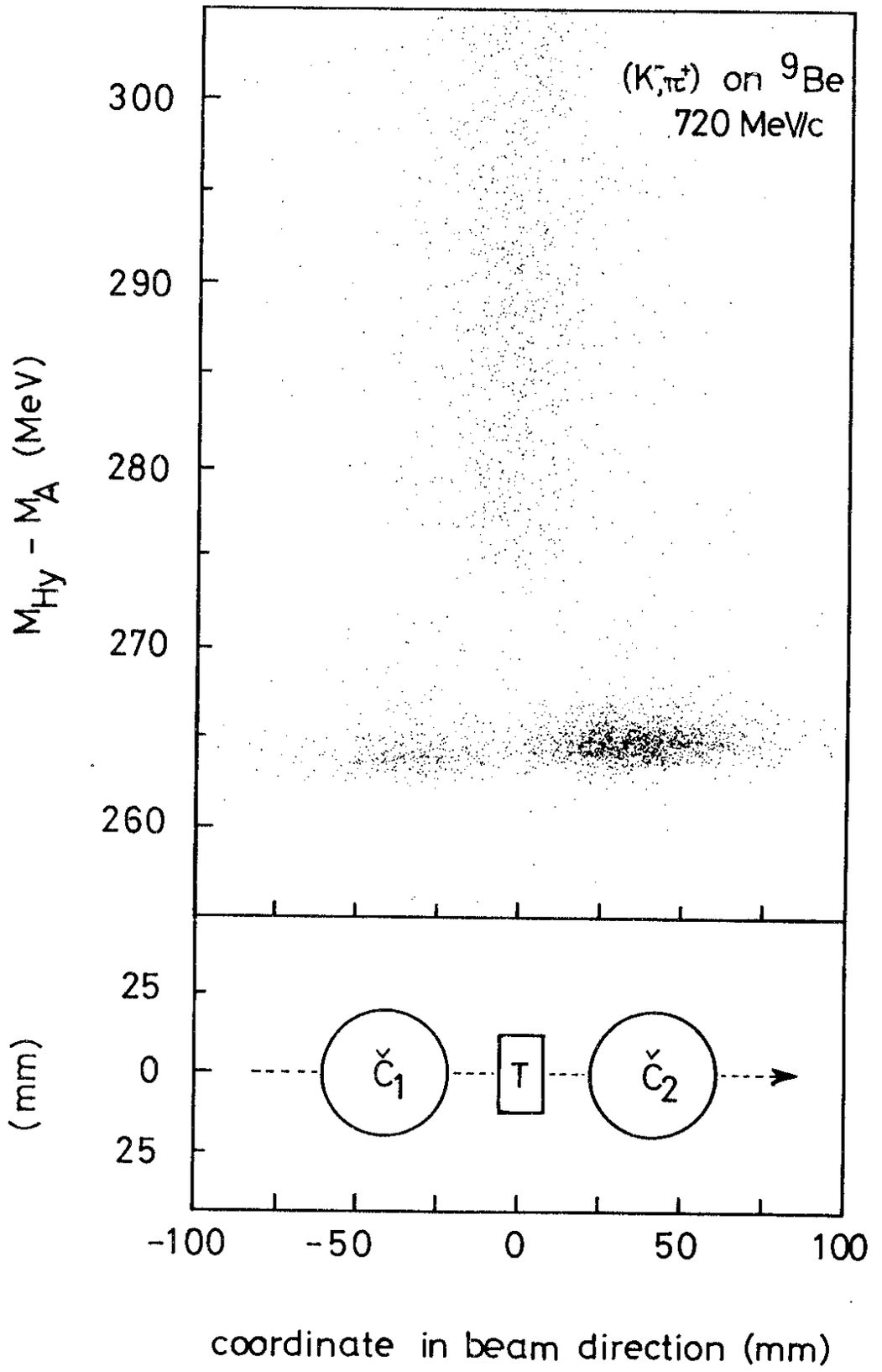
(K⁻,π⁺) on ⁹Be
720 MeV/c
300
290
280
270
260
M_Hy - M_A (MeV)
25
0
25
(mm)
Č1
T
Č2
-100
-50
0
50
100
coordinate in beam direction (mm)

Fig. 3

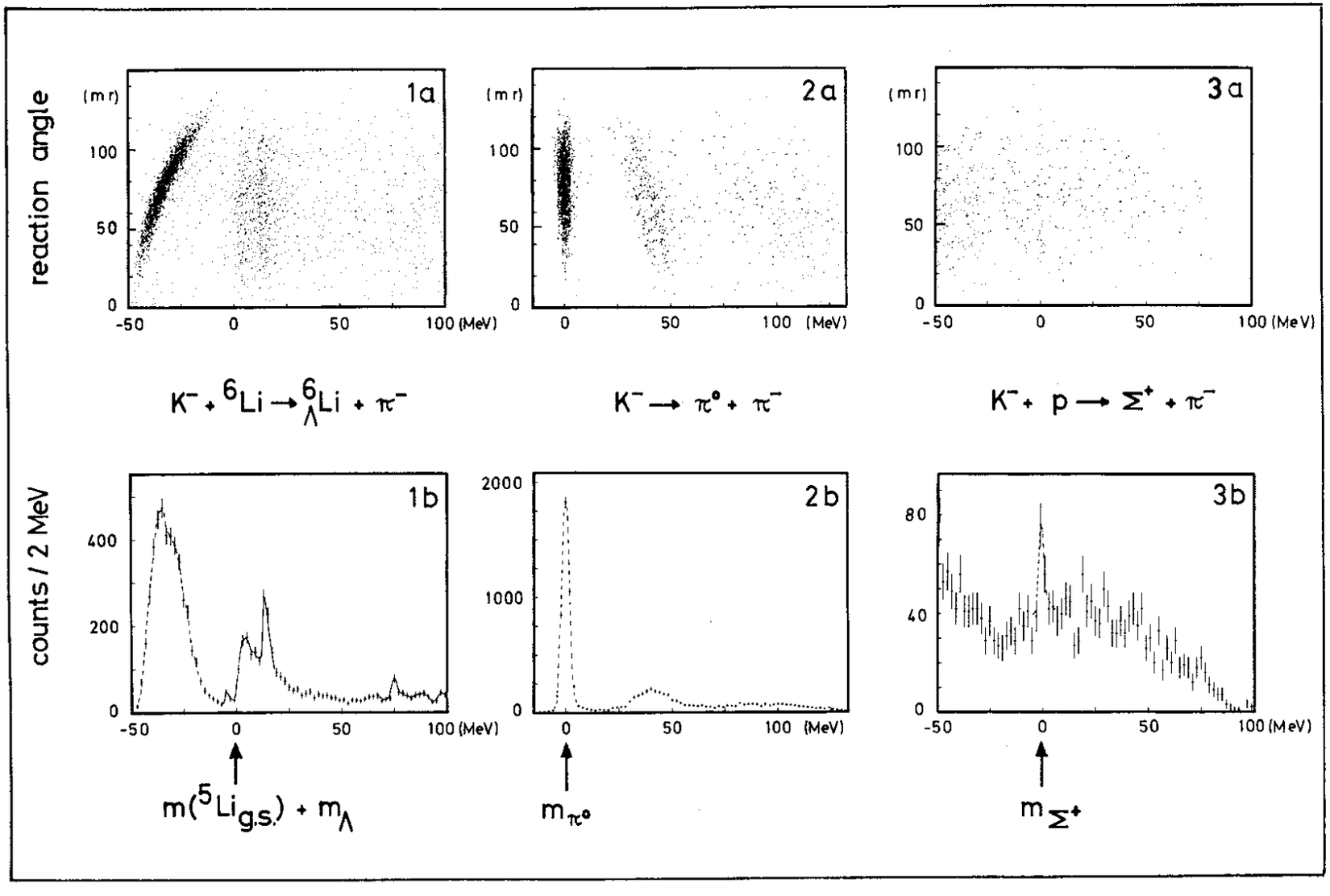
reaction angle
(mr)
100
50
0
1a
-50
0
50
100 (MeV)
2a
3a
$K^- + {}^6Li \rightarrow {}^6_\Lambda Li + \pi^-$
$K^- \rightarrow \pi^0 + \pi^-$
$K^- + p \rightarrow \Sigma^+ + \pi^-$
counts / 2 MeV
400
200
1b
2000
1000
2b
80
40
3b
$m(^5Li_{g.s.}) + m_\Lambda$
m_{π^0}
m_{Σ^+}

Fig. 4

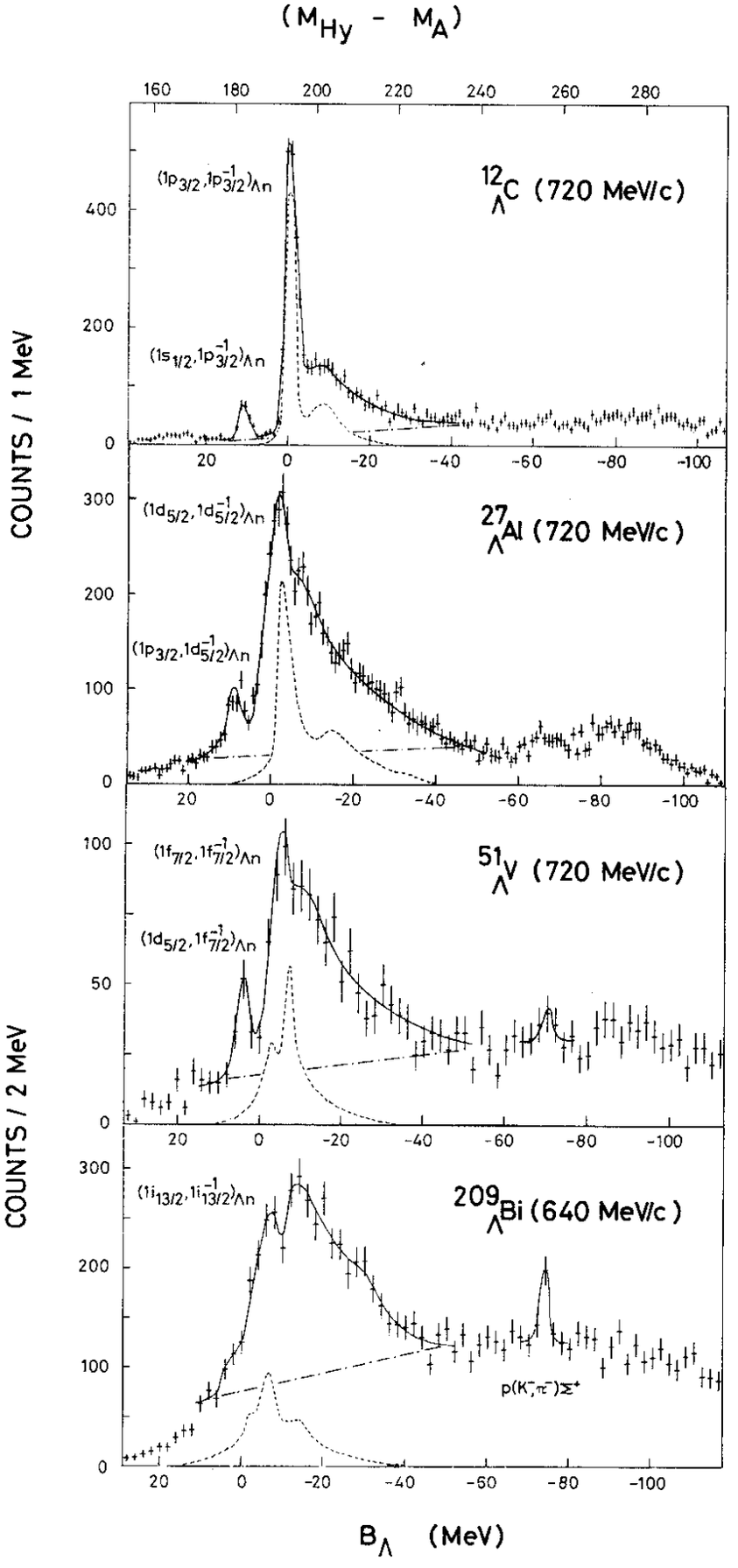
(M_Hy - M_A)
160
180
200
220
240
260
280
(1p3/2,1p3/2^-1)Λn
12ΛC (720 MeV/c)
(1s1/2,1p3/2^-1)Λn
400
200
0
20
0
-20
-40
-60
-80
-100
(1d5/2,1d5/2^-1)Λn
27ΛAl (720 MeV/c)
(1p3/2,1d5/2^-1)Λn
300
200
100
0
(1f7/2,1f7/2^-1)Λn
51ΛV (720 MeV/c)
(1d5/2,1f7/2^-1)Λn
100
50
0
(1i13/2,1i13/2^-1)Λn
209ΛBi (640 MeV/c)
p(K⁻,π⁻)Σ⁺
300
200
100
0
COUNTS / 1 MeV
COUNTS / 2 MeV
BΛ (MeV)

Fig. 5

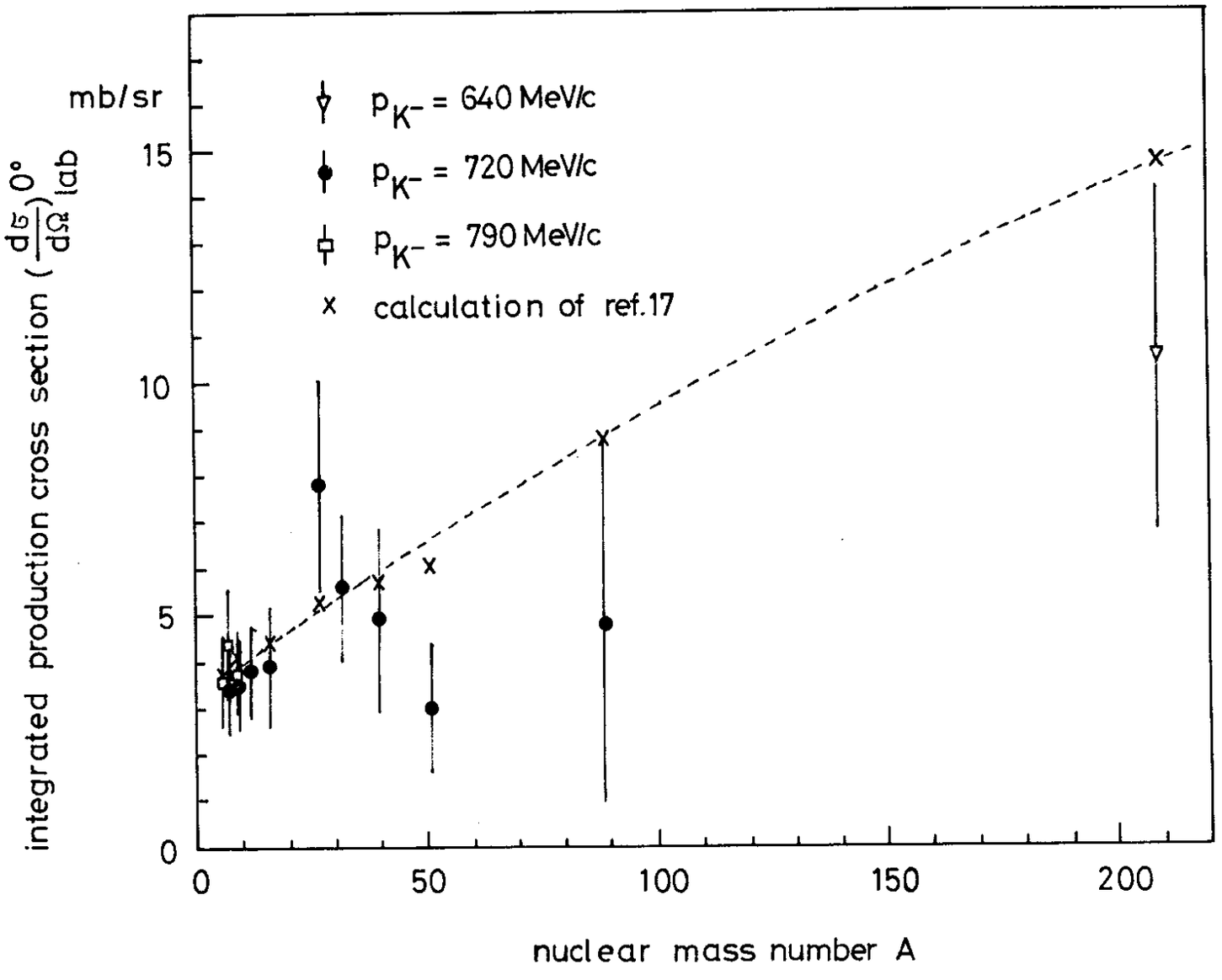
mb/sr
integrated production cross section $(\frac{d\sigma}{d\Omega})^{0°}_{lab}$
p_{K^-} = 640 MeV/c
p_{K^-} = 720 MeV/c
p_{K^-} = 790 MeV/c
x calculation of ref.17
15
10
5
0
0
50
100
150
200
nuclear mass number A

Fig. 6